Astronomy & Astrophysics manuscript no. wd1
February 1, 2008
© ESO 2008

arXiv:0704.3073v1 [astro-ph] 23 Apr 2007

The distance and neutral environment of the massive stellar cluster Westerlund 1

R. Kothes[1,2] and S. M. Dougherty[1]

[1] National Research Council of Canada, Herzberg Institute of Astrophysics, Dominion Radio Astrophysical Observatory, P.O. Box 248, Penticton, British Columbia, V2A 6J9, Canada
[2] Department of Physics and Astronomy, University of Calgary, 2500 University Drive N.W., Calgary, AB, Canada

Received 19 February 2007 / Accepted 13 April 2007

ABSTRACT

Context. In spite of a large number of recent publications about the massive stellar cluster Westerlund 1, its distance from the Sun remains uncertain with values as low as 1.1 kpc, but largely between 4 and 5 kpc.
Aims. The goal of this study is to determine a distance to Westerlund 1 independent of the characteristics of the stellar population and to study its neutral environment, using observations of atomic hydrogen.
Methods. The H I observations are taken from the Southern Galactic Plane Survey to study H I absorption in the direction of the H II region created by the members of Westerlund 1 and to investigate its environment as observed in the H I line emission. A Galactic rotation curve was derived using the recently revised values for the Galactic centre distance of $R_\odot$ = 7.6 kpc, and the velocity of the Sun around the Galactic centre of $\Theta_\odot$ = 214 km s^{-1}. This rotation curve successfully predicts the location of the Tangent point gas and the velocity of the Sagittarius Arm outside the solar circle on the far side of the Galaxy to within 4 km s^{-1}. Compared to the typically used values of $R_\odot$ = 8.5 kpc and $\Theta_\odot$ = 220 km s^{-1} this reduces kinematically determined distances by more than 10 %.
Results. The newly determined rotation model leads us to derive a distance of 3.9 ± 0.7 kpc to Westerlund 1, consistent with a location in the Scutum–Crux Arm. Included in this estimate is a very careful investigation of possible sources of error for the Galactic rotation curve. We also report on small expanding H I features around the cluster with a maximum dynamic age of 600,000 years and a larger bubble which has a minimum dynamic age of 2.5 million years. Additionally we re-calculated the kinematic distances to nearby H II regions and supernova remnants based on our new Galaxic rotation curve.
Conclusions. We propose that in the early stages of the development of Wd 1 a large interstellar bubble of diameter about 50 pc was created by the cluster members. This bubble has a dynamic age similar to the age of the cluster. Small expanding bubbles, with dynamical ages ~ 0.6 Myr are found around Wd 1, which we suggest consist of recombined material lost by cluster members through their winds.

Key words. open clusters and associations: individual (Westerlund 1) – ISM: bubbles – Stars: winds, outflows – H II regions – supernova remnants

1. Introduction

Westerlund 1 (Wd 1) is a highly reddened compact cluster with a large population of post-main sequence massive stars, including OB supergiants and hypergiants, red and yellow supergiants, and Wolf-Rayet (WR) stars (Clark & Negueruela 2002; Clark et al. 2005). The mass of Wd 1 is likely to be in excess of $10^5 M_\odot$ (Clark et al. 2005), exceeding that of any of the other known massive Galactic clusters, including NGC 6303 (Crowther & Dessart 1998), the Arches (Figer et al. 2002) and Quintuplet (Figer et al. 1999), and is more comparable to the mass of Super Star Clusters (SSC), previously identified only in other galaxies. If Wd 1 is indeed a Super Star Cluster within our own Galaxy (Clark et al. 2005), this is a unique opportunity to study the properties of a nearby SSC, where it is possible to resolve the individual massive stars, and determine basic properties more readily than in the typically more distant examples.

In spite of a large number of recent observations of Wd 1, its distance from the Sun remains somewhat uncertain. Piatti et al. (1998) derived a distance of 1.1 ± 0.4 kpc based on photometry of the OB supergiants identified at the time. Using the yellow hypergiants where a spectroscopic luminosity discriminant is available that is lacking for OB supergiants, Clark et al. (2005) determined an upper limit for the distance of 5.5 kpc. Clark et al. (2005) also argue for a lower limit on the distance of 2 kpc based on an analysis of radio continuum data (Clark et al. 1998). They also argue that the comparatively low distance of Piatti et al. (1998) is the result of an error in both the absolute magnitude calibration and the reddening law that was used. Additionally, Clark et al. (2005) did not identify *any* dwarf or giant stars, with all the OB stars being supergiants, unlike the work of Piatti et al. where detection of the main sequence was claimed. Further support for a distance in excess of 2 kpc comes from analysis of near-IR photometry of the WR stars in Wd 1 (Crowther et al. 2006), where the average distance modulus derived from 23 of the 24 known WR stars leads to a distance of 4.7 ± 1.1 kpc. The relatively large uncertainty in this estimate is a result of the uncertainty in the absolute magnitude calibration of WR stars. A more precise estimate of distance comes from an initial analysis of deep IR imaging with the VLT that reveals the main sequence and pre-main sequence populations in Wd 1 from which a photometric distance of 4.0 ± 0.3 kpc is deduced (Brandner et al. 2005).

The most recent analyses appear to be converging on a distance in the range 4-5 kpc. In this paper, we examine H I data in

---

Send offprint requests to: R. Kothes

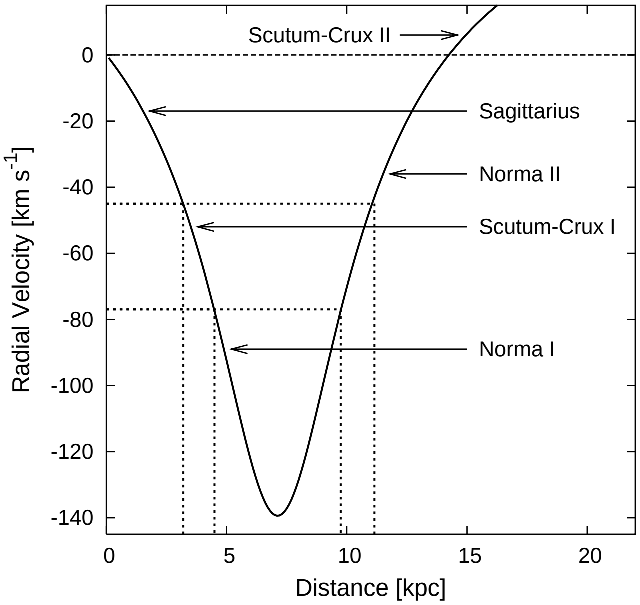

Fig. 1. The Galactic rotation curve toward Galactic longitude of 339°.6 using a Galactocentric radius of $R_\odot = 7.6$ kpc and a circular velocity of $\Theta_\odot = 214$ km s^{-1} for the Sun. We assumed a flat rotation curve and purely circular rotation. The approximate locations of the spiral arms in radial velocity are indicated. Here the indices I and II indicate the first and second time the line of sight passes through that spiral arm (see also Fig. 2).

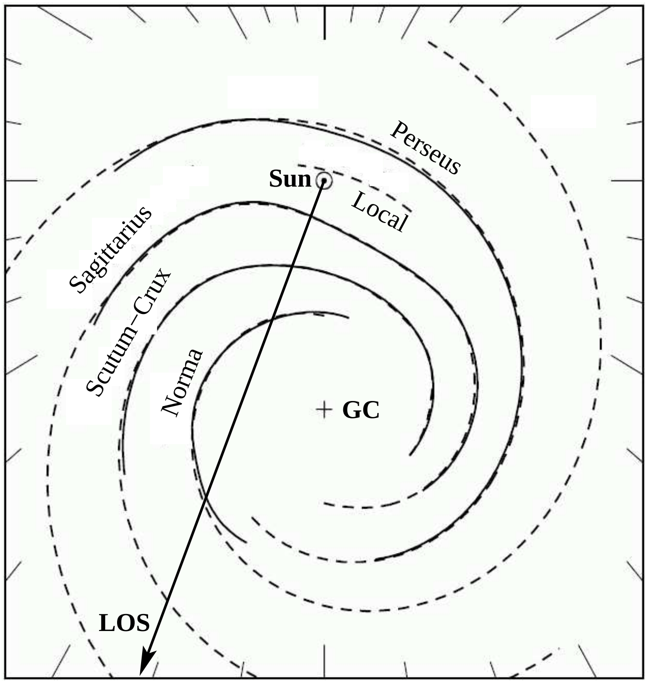

Fig. 2. The spiral arm pattern of the Milky Way Galaxy (Taylor & Cordes 1993; Cordes & Lazio 2002). The names of the spiral arms and the line of sight (LOS) toward Wd 1 are indicated.

the direction of Wd 1 from the Southern Galactic Plane Survey (SGPS) (McClure-Griffiths et al. 2005) to estimate a distance to Wd 1 based on H I absorption and related H I features. We also examine the large-scale distribution of H I in the environment of Wd 1 to search for evidence of the impact of the putative SSC on the surrounding interstellar medium.

2. The SGPS H I data set

The Southern Galactic Plane Survey (McClure-Griffiths et al. 2005) is part of the International Galactic Plane Survey (IGPS), a project devoted to mapping the neutral hydrogen in the plane of the Galaxy, the Milky Way, at arcminute scale. The SGPS maps the region of the Milky Way visible in the southern hemisphere. Other parts of the IGPS are the Canadian Galactic Plane Survey (CGPS, Taylor et al. 2003), which covers the Galactic plane seen in the northern hemisphere, and the VLA Galactic Plane Survey (VGPS, Stil et al. 2006), which connects the two other surveys through the first quadrant of the Milky Way.

The SGPS data were obtained with the Australia Telescope Compact Array (ATCA) and the Parkes 64-m radio telescope. The survey covers an area of $325^{\circ 2}$ from 253° to 358° and 5° to 20° in Galactic longitude and from −1°.5 to +1°.5 in Galactic latitude. In the direction of Wd 1 the total velocity coverage is 600 km s^{-1} from −300 to +300 km s^{-1}. The angular resolution is $\sim 2'$ and the sensitivity ~ 1.6 K.

3. Results

3.1. Galactic kinematics in the direction of Westerlund 1

We carefully investigated the dynamics along the line of sight towards Wd 1. As a starting point we used a flat rotation model to describe the circular rotation in our Galaxy. For this model we have to determine the Galactocentric radius of the Sun $R_\odot$ and its circular velocity around the Galactic centre $\Theta_\odot$. Instead of assuming the standard values, $R_\odot = 8.5$ kpc and $\Theta_\odot = 220$ km s^{-1}, which are still used in most kinematic distance estimates and Galactic models (e.g. Cordes & Lazio 2002), we carefully investigated the literature to find the most recent estimates. $R_\odot$ was determined to be 7.6 ± 0.3 kpc by Eisenhauer et al. (2005) from a high precision measurement of the three dimensional orbit of the star S2, which is orbiting the black hole at the centre of the Galaxy at a distance of less than 0.2″. This is significantly smaller ($\sim$ 11 %) than the previously assumed distance. Feast & Whitelock (1997) determined the angular velocity of circular rotation at the position of the Sun $\Omega_\odot$, from the Oort constants using data from the Hipparcos satellite. $\Omega_\odot = \frac{\Theta_\odot}{R_\odot} = 27.2 \pm 0.8$ km s^{-1} kpc^{-1} gives $\Theta_\odot = 207 \pm 10$ km s^{-1}. Another technique to determine $\Theta_\odot$ is the proper motion of the Galactic Centre. Reid & Brunthaler (2004) found a proper motion of 6.4 mas yr^{-1} for Sagittarius A, which translates to a value of 229 ± 10 km s^{-1} for a distance of 7.6 kpc to the Galactic Centre. Correcting this for the peculiar motion of the Sun, which Reid & Brunthaler (2004) suggest is between 5 and 12 km s^{-1}, we derive $\Theta_\odot = 220 \pm 11$ km s^{-1}. Both values agree within their uncertainties, and averaging the two values we obtain $\Theta_\odot = 214 \pm 7$ km s^{-1}. With these values for $R_\odot$ and $\Theta_\odot$ we can derive the systemic velocity v_{sys} (local standard of rest velocity) measured from the Sun in the direction of Wd 1 as a function of distance (Fig. 1).

We tested our assumption of a flat rotation curve by comparing the measured Tangent point velocity from the SGPS data with the velocity extrapolated from our values for $\Theta_\odot$. The Tangent point at any line of sight through the inner Galaxy is the point at which we look tangential to the circular motion and hence find the largest line of sight velocity. For flat rotation we should observe a radial velocity of −139 km s^{-1} at the Tangent

Table 1. The systemic velocity and distance to the spiral arms along the line of sight toward Wd 1 determined with the Spiral arm model in Fig 2 and the rotation curve in Fig. 1.

Spiral Arm	v_{sys} [km s^{-1}]	d_{lit} [kpc]
Sagittarius I	-17	1.5
Scutum-Crux I	-52	3.5
Norma I	-89	4.9
Norma II	-35	11.5
Scutum-Crux II	+6	15.0
Sagittarius II	+26	18.4

point in the direction of $l = 339.6°$ (Fig. 1). This agrees reasonably well with the observed value of somewhere between -130 km s^{-1} and -135 km s^{-1} (Fig. 3). This is actually a quite remarkable result, since the Tangent point in the direction of Wd 1 is at a distance of about 7 kpc from the Sun at a Galacto-centric radius of about 2.6 kpc. This should be well within the area which is heavily influenced by the central bar of the Milky Way. Benjamin et al. (2005) determined that the central bar has a maximum distance of 4.4 kpc from the Galactic centre, using a Galacto-centric distance of 8.5 kpc for the Sun. With the value of $R_\odot = 7.6$ kpc this would translate to a maximum distance of 3.9 kpc which is significantly higher than the Galactoc-centric distance of the Tangent point.

To determine the distance to the spiral arms in the direction of Wd 1 we utilise the distribution of free electrons in our Galaxy as described in the models of Taylor & Cordes (1993) and Cordes & Lazio (2002). The peaks in electron density indicate the locations of the spiral arms in this direction of the Galaxy (Fig. 2). Since Taylor & Cordes (1993) and Cordes & Lazio (2002) used a Galacto-centric radius of $R_\odot = 8.5$ kpc for the Sun in their spiral arm model, we re-scaled this profile for $R_\odot = 7.6$ kpc. The distances to the nearby H II regions used to define the distance of the nearby spiral arms were derived spectroscopically. Hence, we left the distance to the two nearby spiral arms alone and only re-scaled the distances to the other more distant spiral arms. With the rotation curve in Figure 1, we derive the systemic velocities at the centres of the individual spiral arms. These newly determined distances and systemic velocities are listed in Table 1. A comparison of these values with the H I emission profile in the direction of Wd 1 is shown in Fig. 3.

The locations of the individual spiral arms in velocity space agree remarkably well with the brightness temperature peaks in the H I emission profile (Fig. 3). The emission peak between -140 and -100 km s^{-1} near the Tangent point is produced by a pile up in velocity space rather than a real density enhancement. In this region, the velocity does not change significantly with distance, resulting in one velocity channel containing the emission from H I distributed over a much larger distance interval than in other locations along the line of sight. This creates a peak in the H I emission profile close to the Tangent point velocity. There are two spiral arms that can be seen distinct from the others, Norma I with a centre velocity of -89 km s^{-1} and Sagittarius II, for which the model centre velocity of +26 km s^{-1} is very close to the emission peak at +22 km s^{-1}. Since Sagittarius II is supposed to be well outside the Solar Circle on the other side of the Galaxy in any Galactic model, this agreement with the H I emission profile is incredible and boosts our confidence in our rotation model. The other spiral arms are clumped into two groups: Scutum-Crux I and Norma II merge at a radial velocity of about -40 km s^{-1} and the Local arm, Sagittarius I, and Scutum-Crux II are at low negative velocities.

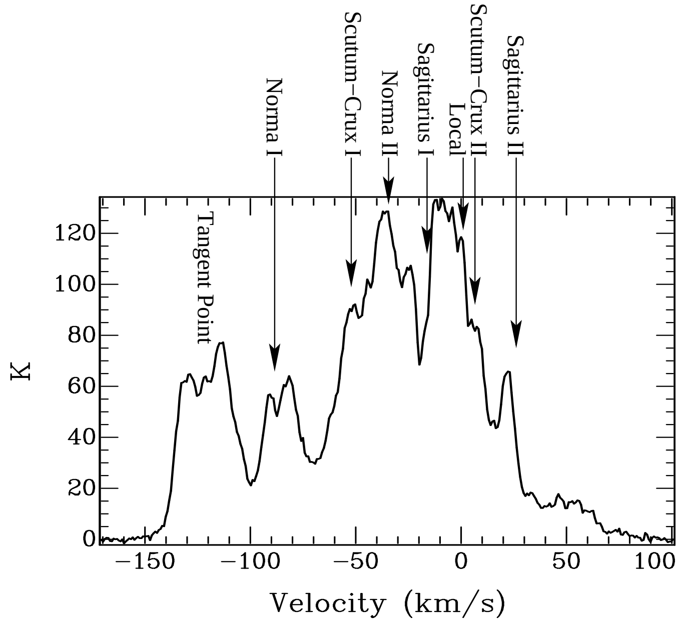

Fig. 3. H I emission profile averaged over an area of a few arcminutes towards Wd 1. The locations of the spiral arms as listed in Table 1 are indicated. The Local arm is indicated at 0 km s^{-1}

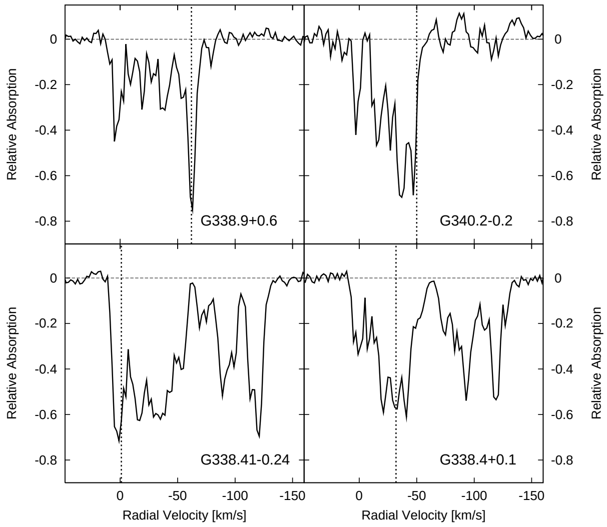

Fig. 4. H I absorption profiles of four radio bright H II regions in the vicinity of Wd 1. To make the individual components better comparable we plotted the relative absorption – the ratio of absorbed emission to total emission – as a function of radial velocity. The dotted vertical lines indicate the systemic velocities of the H II regions (Russeil 2003), which, within their uncertainties, are in excellent agreement with the absorption peaks.

3.2. H I *absorption*

The radio continuum emission of the H II region produced by the Wd 1 cluster is not bright enough at 1420 MHz to produce a prominent H I absorption profile. Its peak brightness temperature is only about 24 K in the SGPS data and the source is barely resolved. Its diameter is about 3′ at a resolution of 2′. Therefore, we have to average over several velocity channels to amplify the weak absorption signal and increase its signal-to-noise ratio. For each spiral arm along the line of sight we tried to average those channels that are likely to produce the deepest absorption.

Table 2. Characteristics of radio bright H II regions and supernova remnants in the vicinity of Wd 1. Column 1 contains a name based on the Galactic coordinates of the object. Columns 2 and 3 contain information about the systemic velocity and derived kinematic distance found in the literature (Russeil 2003). Column 4 contains the distance to the source based on the rotation curve and method described in Sections 3.1 and 4.1, respectively. Column 5 indicates the proposed spiral arm the object resides in.

Source	v_{sys} [km s^{-1}]	d_{lit} [kpc]	d_{new} [kpc]	Spiral Arm
G337.8−0.1			≈ 11	Norma II
G337.95−0.48	−41	3.1	$2.9^{+1.2}_{-0.4}$	Scutum Crux I
G338.0−0.1	−51	12.0	$10.7^{+1.4}_{-0.4}$	Norma II
G338.41−0.24	−1	15.7	$14.0^{+4.5}_{-0.9}$	Scutum-Crux II
G338.4+0.1	−32	13.1	$11.7^{+2.0}_{-0.5}$	Norma II
G338.8+0.6	−62	4.3	$3.9^{+0.9}_{-0.4}$	Scutum-Crux I
G338.5+0.1			≈ 11	Norma II
G338.9−0.1	−38	3.1	$2.8^{+1.2}_{-0.6}$	Scutum-Crux I
G338.9+0.4			≈ 3.9	Scutum-Crux I
G339.13−0.41	−38	3.1	$2.8^{+1.2}_{-0.6}$	Scutum-Crux I
Wd 1	−55		$3.6^{+1.0}_{-0.4}$	Scutum-Crux I
G339.58−0.12	−34	2.8	$2.6^{+1.3}_{-0.7}$	Scutum-Crux I
G339.84+0.27	−20	14.1	$12.5^{+2.7}_{-0.6}$	Norma II
G340.2−0.2	−50	3.7	$3.5^{+1.0}_{-0.5}$	Scutum-Crux I
G340.24−0.48	−61	4.4	$3.9^{+0.9}_{-0.3}$	Scutum-Crux I
G340.6+0.3			≈ 15	Scutum-Crux II

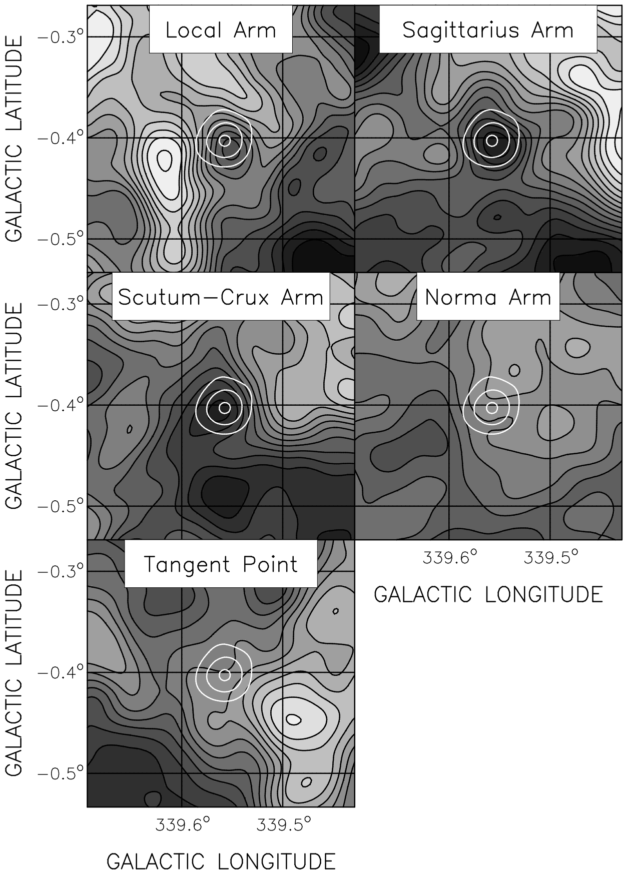

Fig. 5. H I channels images averaged together to demonstrate in which spiral arms Wd 1 is absorbed. For the individual arms we averaged over: +5 to −1 km s^{-1} (Local arm), −10 to −20 km s^{-1} (Sagittarius arm), −32 to −45 km s^{-1} (Scutum-Crux arm), −85 to −102 km s^{-1} (Norma arm), and −110 to −125 km s^{-1} (Tangent Point). In these images white denotes high and black weak emission. The radio continuum emission of Wd 1 is indicated by the white contours.

In these absorption profiles we can identify those velocity intervals in the spiral arms where the H I produces deep and distinct absorption features and those that do not. As a reference we used the absorption profiles of the nearby H II regions shown in Fig. 4. Two of these, representing the G338.9+0.6 and the G340.2−0.4 complexes, are Scutum-Crux I objects according to their systemic velocity (see Table 2). The other two H II regions are located beyond the Tangent point in Norma II (G338.4+0.1 complex) and G338.41-0.24 might even reside in Scutum-Crux II.

The absorption of the three nearby arms, the Local arm, Sagittarius I, and Scutum-Crux I, was identified in the absorption profiles of the two H II regions in Scutum-Crux I since their profiles are not contaminated by absorption of H I located beyond the Tangent point. For Norma I and the Tangent point we used the two H II regions that are located beyond the Tangent point on the other side of the Galaxy. We found distinct absorption in the Local arm between +5 and −1 km s^{-1}, for Sagittarius I between −10 and −20 km s^{-1}, for Scutum-Crux I between −32 and −45 km s^{-1}, for Norma I between −85 and −102 km s^{-1}, and for the Tangent point between −110 and −125 km s^{-1}. For Scutum-Crux I we did not use negative velocities higher than −45 km s^{-1} to avoid confusion with a possible bubble centered at Wd 1 (see section 3.3).

The results of our averaging procedure are shown in Fig 5. It is apparent that the radio continuum emission from Wd 1 is absorbed by the Local arm, Sagittarius I, and Scutum-Crux I. This is indicated by a hole in the distribution of H I emission at the position of Wd 1. There is no evidence for absorption in Norma I or the Tangent point gas. This indicates a location in Scutum-Crux I or at the near edge of Norma I. The latter, however, is rather unlikely, because there must not be any absorbing Norma I material between us and Wd 1. All H II regions shown in Fig. 4 have a very deep distinct absorption feature at their systemic velocity, which is likely created by material in their vicinity in the cloud complex from which the stars in those H II regions were formed. Since the remains of these clouds are expected to be very dense and cold the optical depth should be rather high. This should produce deep absorption lines. If Wd 1 is located in the Norma arm it cannot have such a component. This makes a Scutum-Crux arm location more likely, however, it does not entirely exclude the possibility of a location at the near edge of the Norma arm.

3.3. The neutral environment of Wd 1

We carefully investigated the HI data in the velocity range of the Scutum-Crux arm and at velocities corresponding to the near edge of the Norma arm. We found one prominent feature in velocity space which is exactly centered at the position of Wd 1 at a velocity of -55 km s^{-1}. This feature is shown in Fig 6, indicated by the dashed ellipses (top and right panels). The dashed circle in the centre image marks the location of this expanding bubble projected back to the map plane. This feature, B1, cannot be an absorption feature since the depression visible at the loca-

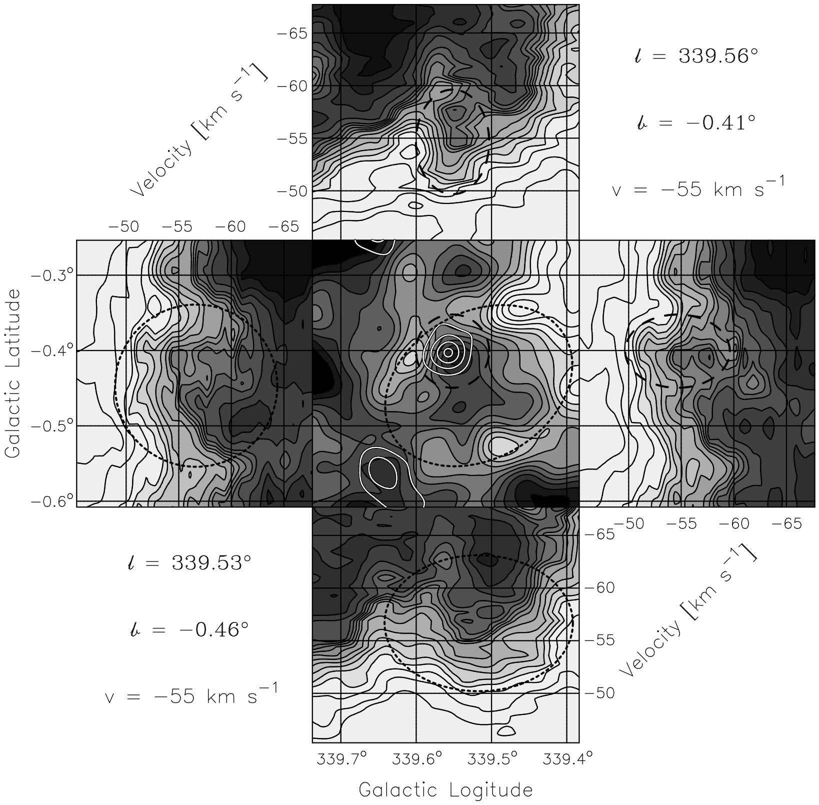

Fig. 6. Three views of the two small expanding bubbles, B1 and B2, around Wd 1, indicated by dashed and dotted ellipses respectively. Longitude-velocity slices are displayed at the top and bottom and the velocity-latitude slices in the left and right panels. The HI channel map at about -55 km/s in longitude-latitude is shown in the centre, with Wd 1 indicated by the white contours. The bright emission in the velocity slices mark the gas at the far edge of Scutum-Crux I. In these images black represents low and white high intensity.

tion of Wd 1 is deeper than the peak brightness of Wd 1's radio continuum emission. In the absorption map of the Scutum-Crux arm (Fig. 5) the velocity interval related to this expanding bubble was omitted to avoid confusion with a hole in the H I map that is created by a lack of H I and not actual H I absorption.

Feature B1 seems to be located at the edge of a much larger elliptical bubble (B2), indicated by the dotted ellipses in Fig. 6. This feature is very obvious in the map plane but is not as clear in velocity space (left and bottom panels of Fig. 6). There are fingers of emission emerging from the bright Scutum-Crux I gas towards higher negative velocities, indicating an expansion for this feature. However, these fingers are not closed in an end cap, which would mark the part of the bubble that is moving towards us. Bubble B1 is closed in velocity space, which makes it very easy to detect. The expansion velocity of B1 is 5 km s^{-1}, as readily seen in Fig. 6. The expansion velocity of B2 is not easy to identify since the end cap is missing, but the velocity fingers seem to indicate a somewhat higher expansion velocity. The spatial coincidence of the two features suggests both are associated with Wd 1, supported by their central velocity of −55 km s^{-1}. This velocity is well within the velocity interval predicted for Wd 1 by the H I absorption measurements. Therefore we adopt a radial velocity of -55 ± 3 km s^{-1} for Wd 1. Uncertainties for the radial velocities along the line of sight are discussed in Sect. 4.1.

At a radial velocity of −55 km s^{-1} a larger field of view reveals a much larger bubble-like feature (B3), which is open to the south, away from the Galactic plane (Fig. 7). The emission associated with Bubble B2 can be seen in the lower right corner of B3. To the north, B3 consists of a shell with two large, bright, and complex emission regions to the east and west. The eastern region contains the H II complex G340.2−0.2, with a radial velocity of −50 km s^{-1} (Table 2). This suggests that Wd 1 and the H II region complex G340.2−0.2 are evolving in the same environment, at the far side of Scutum-Crux I.

4. Discussion

4.1. The distance to Westerlund 1

We determine a radial velocity of -55 ± 3 km s^{-1} for Wd 1 from the central velocity of the bubbles in which we believe it is located. Using the rotation curve determined in Sect. 3.1 (see Fig. 1) this translates to a distance of 3.6 ± 0.2 kpc or 10.6 ± 0.2 kpc. The closer distance is preferable, because the H II region of Wd 1 does not indicate any absorption in the H I gas of Norma I or near the Tangent point. Additionally, the previous distance estimates are $\sim 4-5$ kpc. A comparison with the spiral arm model in Fig. 2 and the calculated distances to the spiral arms in Table 1 reveals that Wd 1 is located in the Scutum-Crux I arm.

A possible source of uncertainty for our rotation curve could be the presence of non-circular motion. Non-circular velocity components due to streaming motion can reach a maximum of about ±10 km s^{-1} (Burton 1972). This would result in ±8 km s^{-1} projected to the line of sight towards Wd 1 assuming a distance of 3.6 kpc. Another source of non-circular motion could be a

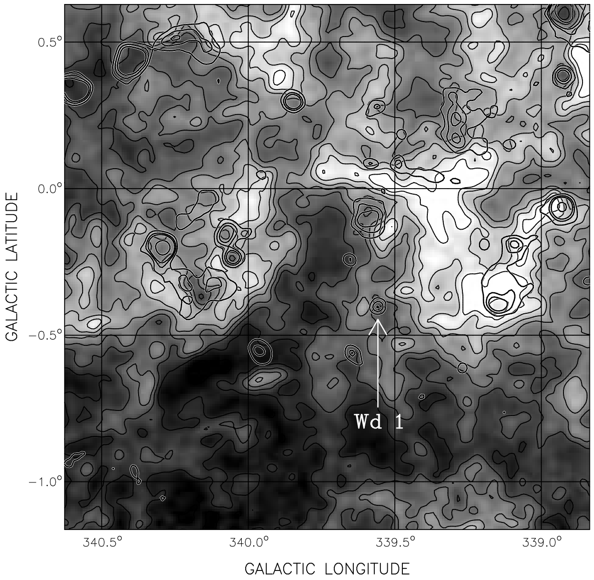

Fig. 7. H I channelmap at a radial velocity of $-55\ \mathrm{km\ s^{-1}}$ from the SGPS. Black contours go from 20 K to 90 K in steps of 10 K. Grayish contours indicate the 1420 MHz continuum emission. The location of Wd 1 is indicated.

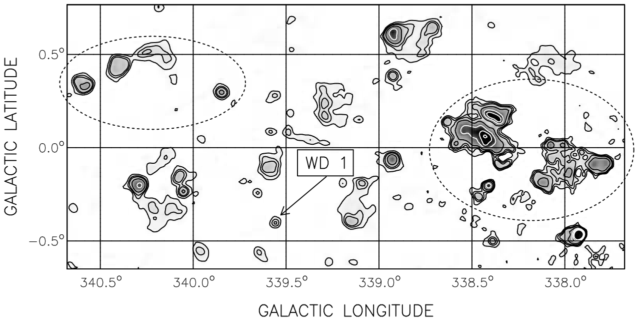

Fig. 8. Radio continuum emission at 1420 MHz around Wd 1 taken from the end channels of the SGPS H I observations. Contours are at 11, 17, 23, and 40 K (black) and 80, 120, and 160 K (white). The dotted ellipses enclose SNRs and H II regions that are believed to be beyond the Tangent point. The location of Wd 1 is indicated.

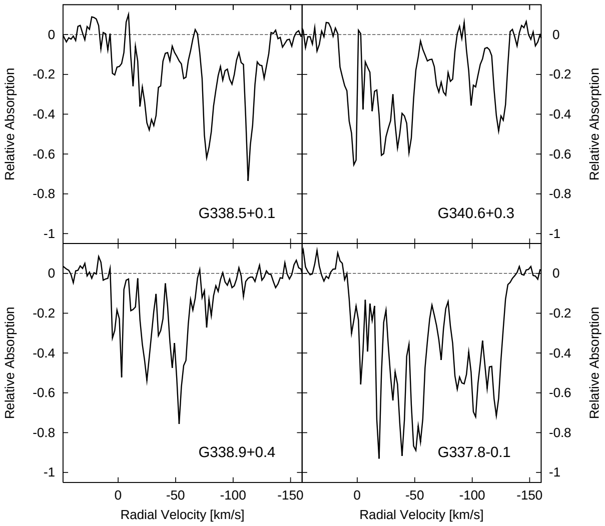

Fig. 9. H I absorption profiles of one radio bright H II region (G338.9+0.4) and three bright SNRs in the vicinity of Wd 1.

spiral shock, which is always directed towards the Galactic centre. At the location of Wd 1 the spiral shock would be directed away from us, leading to an underestimate of the actual distance. Typical values for the velocity shift due to the spiral shock could reach a maximum of 30 km $\mathrm{s^{-1}}$ (Foster & MacWilliams 2006), which would translate to about 24 km $\mathrm{s^{-1}}$ projected to the line of sight. Random motion add another ±5 km $\mathrm{s^{-1}}$ to our uncertainty. Taking all these uncertainties into account, we derive a systemic velocity of -55^{+9}_{-26} km $\mathrm{s^{-1}}$ for Wd 1. In the direction of Wd 1,the velocity versus distance gradient is rather steep (see Fig 1), so the large velocity uncertainty does not translate to a large distance uncertainty. This radial velocity corresponds to a distance of $3.6^{+1.0}_{-0.4}$ kpc, or by choosing the centre of the uncertainty interval as the most probable distance, we get 3.9 ± 0.7 kpc. This result agrees very well with the latest independent distance estimates of 4.0 ± 0.3 kpc (Brandner et al. 2005) and 4.7 ± 1.1 kpc (Crowther et al. 2006). This distance is consistent with a location at the far side of the Scutum-Crux I arm. Furthermore, the bubbles B1 and B2 in Fig. 6 seem to be emerging from the bright gas at the high velocity edge of the Scutum-Crux I arm towards higher negative velocities, supporting a location on the far side of this arm.

4.2. Distance estimates for H II *regions and SNRs in the vicinity of Wd 1*

In Figure 8 we show a 1420-MHz radio continuum image of the area around Wd 1, created from the end-channels of the H I data that do not contain any neutral hydrogen emission. Wd 1 is located in a rich area of radio bright H II regions and supernova remnants. In Table 2 we list H II regions and complexes for which the systemic velocity is known and for which the distance ambiguity in the inner Galaxy, where each radial velocity corresponds to two possible distances, was solved (Russeil 2003). With the rotation curve shown in Fig. 1, new distances to these objects can be deduced. A comparison of the systemic velocities of these H II regions with the centre velocity of each spiral arm, determined in Sect. 3.1 (see Table 1), gives the most likely spiral arm where these objects reside (Table 2). Almost all of these sources are apparently concentrated in the Scutum-Crux I arm and the Norma II arm. Only G338.41 − 0.24 seems to be located even further away in the Scutum-Crux II arm. Objects believed to be beyond the Tangent point are encircled by dashed ellipses in Fig. 8. It is quite curious that no objects were found in either Sagittarius I or Norma I arms

H I absorption profiles for four additional radio bright sources can also be determined (Fig. 9). The distances and systemic velocities of these objects were previously unknown. These absorption profiles were compared with those in Fig 4 to determine the most likely spiral arm location for these objects. We then assume the distance to the centre of that particular spiral arm to be the most likely value for these objects, with uncertainties ∼ ±1 kpc (Table 2).

The absorption profile of the HII region G338.9+0.4 in Fig. 9 is very similar to G338.9 + 0.6 and G340.2 − 0.2 (see Fig. 4) with no evidence of absorption in Norma I or at the Tangent point. This suggests G338.9 + 0.4 could be a part of the G338.9 + 0.6 H II region complex, just to the north (see Fig 8). Therefore, we propose a Scutum-Crux I location at a distance of about 3.9 kpc.

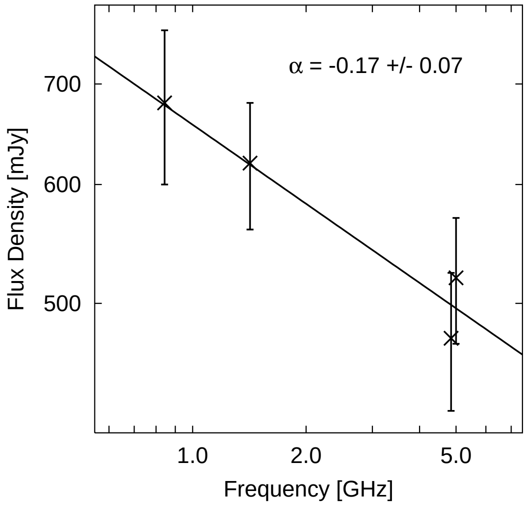

Fig. 10. Radio continuum spectrum of the H ii region, produced by the members of Wd 1.

The SNR G340.6+0.3 is absorbed by Norma I and the Tangent point gas and also shows a deep absorption feature with a relative absorption of almost 0.7 at about 0 km s^{-1} (Fig 9). This makes its absorption profile very similar to that of G338.41−0.24 (Fig 4). No other source shows such a deep and wide absorption feature around a velocity of 0 km s^{-1}. This indicates a location on the other side of the Galaxy in Scutum-Crux II at about 15 kpc. This gives the SNR a diameter of about 26 pc. It is not unusual that absorption features that are far away seem to be deeper than those that are nearby. The reason for this is simply the area probed by the observing beam becomes bigger with distance so that more H i is detected within one beam.

The SNRs G337.8−0.1 and G338.5+0.1 show absorption by Norma I and at the Tangent point but lack the deep and wide absorption feature at 0 km s^{-1}. Their absorption profiles look very similar to that of G338.4+0.1 in Fig. 4. Therefore these two SNRs are most likely Norma II objects at a distance of about 11 kpc. This gives G338.5+0.1 a diameter of about 30 pc and G337.8−0.1 an extent of about 30×20 pc.

4.3. The Wd 1 H ii *region*

We determined radio continuum flux densities for the Wd 1 H ii region at 1.4 GHz (620 ± 60 mJy) from the continuum end channels of the SGPS H i data and at 843 MHz (680 ± 80 mJy) from data of the Molonglo Survey (Green et al. 1999). We added two flux density measurements from the literature at 5 GHz (520 mJy, Haynes et al. 1979) and at 4.85 GHz (474 mJy, Wright et al. 1994) (Fig. 10). Since no error was given for the Haynes et al. (1979) value we weighted both fluxes equally. The error bars plotted in Fig. 10 represent 10% of the flux density. A weighted least-squares fit gives a spectral index of $\alpha = -0.17 \pm 0.07$, that we interpret as arising from optically thin thermal plasma.

The observed diameter of Wd 1 in our 1.4 GHz data is 3.′5 at a resolution of 2′. This results in an actual diameter of 3′. This agrees with its appearance in the 843 MHz Molonglo Survey (Green et al. 1999). The observed peak of the radio continuum emission is about 24 K. Correcting for the synthesised beam, the H ii region has a peak brightness temperature of 33 K at 1.4 GHz. The observed brightness temperature T_B at frequency ν is related to the electron temperature T_e inside the H ii region and the optical depth τ by:

$$T_b(\nu) = T_e\,(1 - e^{-\tau(\nu)}), \tag{1}$$

where the optical depth at frequency ν is given by:

$$\tau(\nu) = 8.235\,10^{-2} \left(\frac{T_e}{\mathrm{K}}\right)^{-1.35} \left(\frac{\nu}{\mathrm{GHz}}\right)^{-2.1} \left(\frac{EM}{\mathrm{pc\,cm^{-6}}}\right). \tag{2}$$

(e.g. Rohlfs & Wilson 2004). Here EM is the emission measure related to the path length l through the H ii region and the electron density n_e inside it by:

$$EM = \int n_e^2\,dl \tag{3}$$

With an electron temperature of $T_e = 8000 \pm 2000$ K and a path length of 3.5 pc (3′ at 3.9 kpc) through the H ii region, we estimate an optical depth of $0.0041^{+0.0014}_{-0.0008}$ and an emission measure of $19000^{+8000}_{-6000}\,\mathrm{pc\,cm^{-6}}$. Hence, $n_e = 74 \pm 13\,\mathrm{cm^{-3}}$ and the total mass of the ionized gas inside the H ii region is $53 \pm 9\,M_\odot$. The frequency at which this emission becomes optically thick (i.e. $\tau_\nu = 1$) is ≈ 100 MHz.

Alternatively, the electron density of the H ii region can be calculated from the observed flux density. For an optically thin Maxwellian plasma, the flux S_ν is given by:

$$S_\nu = 5.7\,10^{-56}\,T_e^{-0.5}\,g_{ff}\,E_V\,d^{-2}\ \mathrm{mJy}, \tag{4}$$

where g_{ff} is the Gaunt-factor defined by:

$$g_{ff} = \frac{\sqrt{3}}{\pi}\left(17.7 + ln\left(\frac{T_e^{1.5}}{\nu}\right)\right) \tag{5}$$

and E_V is the volume emissivity:

$$E_V = \int n_e^2 dV. \tag{6}$$

The radio spectrum in Fig. 10 indicates that the emission is optically thin over the entire observed frequency range. Using the flux density at 843 MHz, we derive an electron density of $n_e = 65 \pm 7\,\mathrm{cm^{-3}}$ and a total ionized mass of $M = 47 \pm 5\,M_\odot$. This is in excellent agreement with the value derived from the observed brightness temperature.

4.4. Wd 1 and its neutral environment

In Section 3, two small (B1 and B2) and one large (B3) bubble in the H i data were described. We believe these are related to Wd 1. The determination of the mass of atomic material in these bubbles is difficult since these objects, in particular bubble B3, seems to merge with the surrounding ISM in the H i images (Figs. 6 and 7). Bubble B1 and B2 together contain a mass of about 300 $M_\odot$ with an error of at least 50 %, assuming the H i is optically thin and the mass ratio between hydrogen and helium is 10:3. The inner edge of bubble B1 seems to be just outside the Wd 1 H ii region (see Fig. 6) giving a diameter of about 5 pc at a distance of 3.9 kpc. At the same distance, bubble B2 has an extent of about 18×10 pc. McClure-Griffiths et al. (2002) defined the dynamic age of a stellar wind bubble that expands as $\propto t^{0.3}$ by:

$$t_6 = 0.29\,\frac{R}{v_{exp}}, \tag{7}$$

where t_6 is the dynamic age of the bubble in Myr, R the radius in pc, and v_{exp} the expansion velocity in km s^{-1}. For bubble B2 the maximum expansion radius calculated from the position of Wd 1 is about 10 pc. If we use an expansion velocity of 5 km s^{-1} for B2, determined for bubble B1, we derive a dynamic age of about 600,000 yr for B2. Since its structure in velocity space (see Fig. 6) implies a somewhat higher expansion velocity than that for bubble B1 and the radius is a maximum expansion radius, this age represents an upper limit.

Crowther et al. (2006) determined an age of 4.5 – 5.0 Myrs for Wd 1, based on the ratio of WR stars to red and yellow hypergiants. Clearly, bubbles B1 and B2 cannot be the stellar wind bubble produced in the early evolution of Wd 1; they are simply too young. Both B1 and B2 could have been created after the last supernova explosion pushed away all material inside the stellar wind bubble. The recent discovery of the X-ray pulsar CXO J164710.2-455216 inside Wd 1 implies that at least one supernova explosion occured inside Wd 1 (Muno et al. 2006). In this case we speculate that B1 and B2 originate from the only source of matter and energy left after the last supernova occurred, the combined winds and mass loss of the cluster stars. In that scenario, the gas in the shells of those bubbles must consist mostly of recombined material previously ejected by the stars in their winds, since the supernova shock wave should have removed any remaining material in the ambient medium. This would imply that the last supernova explosion happened less than 600,000 yr ago. Additionally, the ionized material inside the H II region would also be material ejected by the stars in their winds. The total mass of the ionized gas plus the B2 H I shell is $\sim$ 350 $M_\odot$. If we assume these structures are 500,000 yr old we require 70 stars with an average mass-loss rate of 10^{-5} $M_\odot$ yr^{-1} for each star, which is highly feasible for the stellar population in Wd 1.

We suspect that the impact of the original stellar wind bubble, created by the members of Wd 1 in their early stage of evolution, is represented by bubble B3 (Fig. 7). Its diameter is about 50 pc at a distance of 3.9 kpc. The location of Wd 1 in the lower right corner of this feature is likely the result of a highly structured environment. To the South, away from the Galactic plane, the density is expected to decrease in which case the winds of the members of Wd 1 pushed the material away from the Galactic plane into the Galactic halo. To the West we find a dense cloud complex that impeded free expansion, whereas to the East the winds of the stars pushed material into the cloud centered at the G340.2 – 0.2 H II region complex. In Fig. 8 we can identify three bright compact radio sources that belong to this complex at positions (l,b): (340.3,-0.2), (340.1,-0.15), and (340.1,-0.25). These are all sources with far infrared colours characteristic of ultra-compact H II regions, which are known to be regions of OB star formation (Bronfman et al. 1996). This indicates that the G340.2-0.2 H II region complex is younger than Wd 1 and its formation may well have been triggered by the interaction of the early Wd 1 stellar wind or a supernova explosion with the clouds in which G340.2-0.2 is embedded.

To the North of bubble B3 we find a shell that might still be expanding. Since this shell is the only dynamic feature we observe, we use its distance of 45 pc from Wd 1 as the expansion radius. We do not see any expansion of B3 in the velocity slices of our H I data. If we assume that the dynamic age of bubble B3 equals the assumed age of Wd 1, an expansion velocity of about 3 km s^{-1} is implied, which is a reasonable value. Bubble B3 is certainly much older than B2 and B1, because it is many times as large and a low velocity is indicated by the absence of any visible feature in the velocity slices. Unfortunately we cannot estimate the mass of the bubble because of the confusion with the emission regions to the east and the west.

5. Summary

Based on H I observations from the SGPS, we have established that Wd 1 is in the Scutum-Crux arm of the Galaxy. We find three large bubbles in which Wd 1 is located at a radial velocity of -55^{+9}_{-26} km s^{-1}. Using a flat rotation model of the Galaxy and adopting a galacto-centric distance of 7.6 kpc (Eisenhauer et al. 2005) and a velocity of 214 ± 7 km s^{-1} for the Sun around the Galactic Centre, we transpose the radial velocity of the bubble features to a distance of 3.9 ± 0.7 kpc at a Galacto-centric radius of about 4.2 kpc. We are confident in our derived distance-velocity calibration in this direction, since it predicts to within ±4 km s^{-1} the velocity of the Tangent point and the velocity of the H I gas in the Sagittarius Arm outside the Solar Circle on the far side of the Galactic Centre. Moreover, this is very encouraging since it is believed that the position of Wd 1 is in the region of the Galactic bar.

A distance of 3.9 ± 0.7 kpc is somewhat less than the earlier estimate of 4.7 ± 1.1 kpc based on the absolute magnitude calibration of WR stars (Crowther et al. 2006), but very similar to the 4.0 ± 0.3 kpc determined by Brandner et al. (2005) from initial analysis of the photometric detection of the main and pre-main sequence populations in Wd 1. Though the uncertainty on these estimates is relatively large ($\sim 10-25\%$), a weighted average of these values gives us confidence that the distance to Wd 1 is $\sim$ 4 kpc. Until the final analysis of the photometric observations described in Brandner et al. (2005) is available, we argue that this represents the best distance estimate to Wd 1.

A study of the H I images from the vicinity of Wd 1 revealed three bubble-like features B1, B2, and B3. We believe that bubbles B1 and B2 are the result of the stellar winds of the members of Wd 1 and contain recombined wind material. We argue bubble B3 represents the stellar wind bubble created in the early history of Wd 1. The formation of the H II region complex G340.2−0.2 which is embedded in the eastern edge of B3 may have been triggered by the interaction of the Wd 1 wind with the dense clouds in this area. If this is true, the Wd 1 G340.2−0.2 pair would be a nice example of sequential star formation.

Acknowledgements. We wish to thank Naomi McClure-Griffiths for her help with the SGPS HI and continuum data. We also wish to thank Tom Landecker for careful reading of the manuscript. The Dominion Radio Astrophysical Observatory is a National Facility operated by the National Research Council Canada.

References

Benjamin, R. A., Churchwell, E., Babler, B. L., et al. 2005, ApJ, 630, L149
Brandner, W., Clark, S., & Waters, R. 2005, in Protostars and Planets V, 8344
Bronfman, L., Nyman, L.-A., & May, J. 1996, A&AS, 115, 81
Burton, W. B. 1972, A&A, 19, 51
Clark, J. S., Fender, R. P., Waters, L. B. F. M., et al. 1998, MNRAS, 299, L43
Clark, J. S. & Negueruela, I. 2002, A&A, 396, L25
Clark, J. S., Negueruela, I., Crowther, P. A., & Goodwin, S. P. 2005, A&A, 434, 949
Cordes, J. M. & Lazio, T. J. W. 2002, ArXiv Astrophysics e-prints
Crowther, P. A. & Dessart, L. 1998, MNRAS, 296, 622
Crowther, P. A., Hadfield, L. J., Clark, J. S., Negueruela, I., & Vacca, W. D. 2006, MNRAS, 372, 1407
Eisenhauer, F., Genzel, R., Alexander, T., et al. 2005, ApJ, 628, 246
Feast, M. & Whitelock, P. 1997, MNRAS, 291, 683
Figer, D. F., McLean, I. S., & Morris, M. 1999, ApJ, 514, 202
Figer, D. F., Najarro, F., Gilmore, D., et al. 2002, ApJ, 581, 258
Foster, T. & MacWilliams, J. 2006, ApJ, 644, 214
Green, A. J., Cram, L. E., Large, M. I., & Ye, T. 1999, ApJS, 122, 207

Haynes, R. F., Caswell, J. L., & Simons, L. W. J. 1979, Australian Journal of Physics Astrophysical Supplement, 48, 1
McClure-Griffiths, N. M., Dickey, J. M., Gaensler, B. M., & Green, A. J. 2002, ApJ, 578, 176
McClure-Griffiths, N. M., Dickey, J. M., Gaensler, B. M., et al. 2005, ApJS, 158, 178
Muno, M. P., Clark, J. S., Crowther, P. A., et al. 2006, ApJ, 636, L41
Piatti, A. E., Bica, E., & Claria, J. J. 1998, A&AS, 127, 423
Reid, M. J. & Brunthaler, A. 2004, ApJ, 616, 872
Rohlfs, K. & Wilson, T. L. 2004, Tools of radio astronomy (Tools of radio astronomy, 4th rev. and enl. ed., by K. Rohlfs and T.L. Wilson. Berlin: Springer, 2004)
Russeil, D. 2003, A&A, 397, 133
Stil, J. M., Taylor, A. R., Dickey, J. M., et al. 2006, AJ, 132, 1158
Taylor, A. R., Gibson, S. J., Peracaula, M., et al. 2003, AJ, 125, 3145
Taylor, J. H. & Cordes, J. M. 1993, ApJ, 411, 674
Wright, A. E., Griffith, M. R., Burke, B. F., & Ekers, R. D. 1994, ApJS, 91, 111